

Neural ODEs for holographic transport models without translation symmetry

Zhuo-Fan Gu¹, Yu-Kun Yan², and Shao-Feng Wu^{1,3}

¹*Department of physics, Shanghai University, Shanghai, 200444, China*

²*School of Physics, University of Chinese Academy of Sciences, Beijing, 100049, China*

³*Center for Gravitation and Cosmology, Yangzhou University, Yangzhou 225009, China*

E-mail: guzhuofan@shu.edu.cn, yanyukun20@mails.ucas.ac.cn,
sfwu@shu.edu.cn

ABSTRACT: We investigate the data-driven holographic transport models without translation symmetry, focusing on the real part of frequency-dependent shear viscosity, $\eta_{\text{re}}(\omega)$. We develop a radial flow equation of the shear response and establish its relation to $\eta_{\text{re}}(\omega)$ for a wide class of holographic models. This allows us to determine $\eta_{\text{re}}(\omega)$ of a strongly coupled field theory by the black hole metric and the graviton mass. The latter serves as the bulk dual to the translation symmetry breaking on the boundary. We convert the flow equation to a Neural Ordinary Differential Equation (Neural ODE), which is a neural network with continuous depth and produces output through a black-box ODE solver. Testing the Neural ODE on three well-known holographic models without translation symmetry, we demonstrate its ability to accurately learn either the metric or mass when given the other. Additionally, we illustrate that the learned metric can be used to predict the derivative of entanglement entropy S with respect to the size of entangling region l .

Contents

1	Introduction	2
2	Holographic flow equation	4
3	Machine learning algorithm	6
3.1	Neural ODE	6
3.2	Loss function and inductive bias	7
4	Holographic models	8
4.1	Massive gravity	8
4.2	Linear axions	9
4.3	Generalized axions	10
5	Conclusion and discussion	11
A	From shear response to shear viscosity	14
B	Training scheme and report	17
C	At low temperatures	19
D	Entanglement entropy	21

1 Introduction

The AdS/CFT correspondence is an elegant holographic mapping that brings illuminating insights into quantum gravity and provides fruitful phenomenal models of strongly coupled quantum many-body systems [1, 2]. The standard approach to the holographic modeling involves positing a bulk action, solving the Einstein equation to derive the bulk metric, and then using the holographic dictionary to transform various gravitational observables into field-theory observables. However, constructing a suitable action from a phenomenological perspective is a fundamental and challenging inverse problem in theoretical physics. In addition to relying on the symmetry principle, it usually requires deep domain knowledge and intuition from human experts.

In certain conditions within the realm of holography, some field-theory observables can be derived directly from the bulk metric without necessitating the complete action. This leads to a reduced inverse problem: Can we reconstruct the bulk metric from these field-theory observables? This question is central to an important branch of the broader bulk reconstruction project [3–5], which ambitiously aims to reorganize the degrees of freedom in the CFT into local gravitational physics under specific limits. There are many different methods for reconstructing the bulk metric, part of which can be found in [6–27]. Among others, Hashimoto et al. propose an intriguing scheme using the neural network and deep learning (DL) [28]. They discretize the Klein-Gordon equation for a scalar field in curved spacetime into the architecture of a neural network. The data they use comprises the expectation value of the operator and its conjugate source, with the IR behavior of the field serving as labels. Under the inductive bias that the metric should be smooth, they design a regularization term to guide the training process. After training, the bulk metric is encoded as the weights of the neural network. This scheme is termed the AdS/DL correspondence. It has been quickly applied to construct holographic QCD models and produced interesting outcomes, such as extracting novel features from lattice data on chiral condensate, predicting reasonable masses for excited-state mesons, and deriving the explicit form of a dilaton potential [29–31].

In addition to QCD, holographic models have found extensive applications in condensed matter physics, hydrodynamics, and quantum information. Notably, transport phenomena, such as momentum and charge transports, are considered very suitable for the holographic research based on the bottom-up setup. In this context, Yan et al. propose a data-driven holographic transport model [32]. Their data are the complex frequency-dependent shear viscosity and the network architecture corresponds to the discretization of a radial flow equation. Since the IR solution of the flow equation is fully determined by regularity, the forward propagation of information is designed from IR to UV. Compared to previous algorithms, this design eliminates the need for additional IR labels, reducing systematic errors in the analysis. Recently, a similar algorithm has been developed to learn from optical conductivity [33], which has the potential applications in condensed matter physics, such as strange metal and high-temperature superconductivity.

All the aforementioned works on AdS/DL share a common feature: the emergent extra dimension corresponds to the depth of the neural network. In fact, the neural network itself

is regarded as a bulk spacetime. However, since the neural network has discrete layers, both the spacetime metric and the equation of motion are discretized. This leads to intrinsic discretization errors in the algorithm. Additionally, the regularization term used to induce smooth metrics increases both arbitrariness and computational cost.

To address these discretization problems, Neural ODEs have been introduced for AdS/DL [34–36]. This is a relatively new family of deep neural network models that generalize the standard layer-to-layer propagation to continuous-depth models [37]. In essence, Neural ODEs employ a neural network to parameterize the derivative of the hidden state, while the output is computed using a black-box adaptive differential equation solver. The application of Neural ODEs in holographic modeling, as highlighted in [34], showcases the potential of AI as more than just a data processing tool in theoretical physics, but also as a valuable aid in scientific discoveries.

The purpose of this paper is twofold. On a technical level, we aim to replace the discrete architecture in [32] with Neural ODEs. Note that the metric ansatz was limited to a polynomial in [34–36], which constrains the representation capability of Neural ODEs. In this work, we will eliminate this constraint by incorporating the neural network into the ansatz. It should be pointed out that switching from polynomials to neural networks increases the training difficulty significantly. Fortunately, we find an effective training method. The key strategies include using multiple optimizers in sequence, as well as employing a larger number of initial values and the early-stopping technique to prevent Neural ODEs from getting stuck with bad parameters. On a physical level, we intend to break the translation symmetry that is respected by the theoretical framework in [32]. The latter is indispensable to describe the real-world condensed matter. However, the breaking of translation symmetry presents an important challenge. Following the spirit of AdS/DL, one would expect the framework of the theory to be as universal as possible, so that the machine has the potential to learn novel metrics from the data of field theories, where the gravity dual may not be explicit. In [28], the universality is achieved under the probe limit, where the bulk action generating the background metric can be entirely unknown. In [32], the probe limit is not invoked, but the universality depends heavily on the relationship between the shear viscosity of the boundary field theory and the shear response on the UV boundary. If the translation symmetry is broken, this relationship usually no longer holds. In this work, through a careful analysis of the UV behavior related to the holographic renormalization [38, 39], we find that the shear viscosity and the shear response on the boundary usually have the same real part, even if the translation symmetry is broken. This crucial observation motivates us to use only the real part of the shear viscosity as the training data¹.

Once the data is prepared, we will define our learning tasks. Following [40], we will focus on the holographic models that break translation symmetry but maintain homogeneity

¹It is instructive to note that the shear viscosity does not have the hydrodynamic interpretation when the translation symmetry is broken, but it still quantifies the entropy production rate due to the strain [40]. In fact, the definition of the viscosity tensor is independent with the hydrodynamics: it is the linear response of the stress tensor under a time-dependent deformation [41]. Recent studies on the viscosity for the systems without translation symmetry can be found, e.g., in [42, 43].

and isotropy in geometry. In many of these models, we will demonstrate that the real part of the frequency-dependent shear viscosity is determined exclusively by functions of the bulk metric and the graviton mass. As a reverse engineering, our objective is to investigate whether Neural ODEs can learn one of these functions when the other is given².

The rest of this paper is organized as follows. In Section 2, we will develop a radial flow equation for a large class of the holographic models without translation symmetry. In Section 3, we will introduce the machine learning algorithm, including the architecture, loss function and inductive bias. In Section 4, we will generate the data and display the training results based on three well-known holographic models without translation symmetry. The conclusion and discussion will be presented in Section 5. Additionally, there are four appendices. In Appendix A, we will establish the relationship between the shear viscosity and the shear response. In Appendix B, we will provide the training scheme and report. In Appendix C, we will improve the performance of Neural ODEs at low temperatures. In Appendix D, we will study the entanglement entropy (EE) on the boundary using the bulk metric learned by Neural ODEs.

2 Holographic flow equation

Consider a strongly coupled field theory that is holographically dual to the 3+1 dimensional Einstein gravity minimally coupled with the matter. Suppose that it allows a planar black hole solution, which is described by the line element

$$ds^2 = -g_{tt}(r)dt^2 + g_{rr}(r)dr^2 + g_{xx}(r)d\vec{x}^2, \quad (2.1)$$

and sourced by the energy-momentum tensor

$$T_{\mu\nu} = \text{diag}(T_{tt}(r), T_{rr}(r), T_{xx}(r), T_{xx}(r)). \quad (2.2)$$

Importantly, eq. (2.1) and eq. (2.2) are homogeneous and isotropic along the field theory directions, although we have not assumed that the matter fields are homogeneous. When the black hole is perturbed by the time-dependent shear mode $\delta g_{xy} = g_{xx}h(r)e^{-i\omega t}$, the wave equation has a general form [40]³

$$\frac{1}{\sqrt{-g}}\partial_r(\sqrt{-g}g^{rr}\partial_r h) + (\omega^2 g^{tt} - m^2)h = 0, \quad (2.3)$$

where m is the radially varying graviton mass

$$m(r)^2 = g^{xx}T_{xx} - \frac{\delta T_{xy}}{\delta g_{xy}}, \quad (2.4)$$

²Since there is a trade-off between metric and mass in determining shear viscosity, we do not attempt to learn the two functions simultaneously.

³Here we have assumed that this mode decouples from other perturbations. Since δg_{xy} transforms as a parity-even tensor mode under the rotation in $x - y$ plane, this assumption is quite general. However, one can find a counterexample in the Einstein- $SU(2)$ theory [44], where the coupling appears from a particular background that locks the symmetries in spacetime and $SU(2)$ vector space.

and the Newton constant has been set as $16\pi G_N = 1$. Note that the nonzero graviton mass in the bulk is dual to the breaking of the translation symmetry on the boundary [45].

Consider the bulk spacetime sliced along the radial direction and introduce the shear response function at each slice

$$\chi = \frac{\Pi}{i\omega h}, \quad (2.5)$$

where $\Pi = -\sqrt{-g}g^{rr}\partial_r h$ is the momentum conjugate to the field h in the Hamiltonian formulation. Using eq. (2.5), one can rewrite the wave equation as

$$\partial_r \chi - i\omega \sqrt{\frac{g_{rr}}{g_{tt}}} \left(\frac{\chi^2}{g_{xx}} - g_{xx} \right) + \frac{1}{i\omega} \sqrt{g_{tt}g_{rr}} g_{xx} m^2 = 0, \quad (2.6)$$

which is a radial flow equation of the shear response.

Observing the flow equation (2.6), one can see that the regularity of the shear response indicates

$$\chi(r_h) = g_{xx}(r_h), \quad (2.7)$$

where r_h is the horizon radius. Using eq. (2.7) as the IR boundary condition, the flow equation can be solved to obtain the complex shear response at UV. However, this shear response does not generally represent the desired shear viscosity on the boundary field theory. Nevertheless, through a careful UV analysis in Appendix A, we will demonstrate that for a wide range of theories, their real parts are indeed the same:

$$\eta_{\text{re}}(\omega) = \chi_{\text{re}}(\omega)|_{r \rightarrow \infty}. \quad (2.8)$$

We emphasize that this nontrivial observation is crucial to the theoretical framework of our data-driven model.

To proceed, we will exploit the scaling symmetry of this system

$$r \rightarrow r\lambda, (t, x, y) \rightarrow (t, x, y)/\lambda, g_{rr} \rightarrow g_{rr}\lambda^{-2}, g_{tt} \rightarrow g_{tt}\lambda^2, g_{xx} \rightarrow g_{xx}\lambda^2, \quad (2.9)$$

which indicates that one can set $r_h = 1$ for convenience.

We will further simplify the metric (2.1) by imposing $g_{tt}g_{rr} = 1$ and setting $g_{xx} = r^2$. Then the metric ansatz can be written as

$$ds^2 = -r^2 f(r) dt^2 + \frac{1}{r^2 f(r)} dr^2 + r^2 d\vec{x}^2. \quad (2.10)$$

Replacing the radial coordinate with $z = 1/r$, one can see that the horizon is located at $z_h = 1$ and the boundary at $z_b = 0$. Accordingly, the flow equation (2.6) can be reduced to⁴

$$\partial_z \chi + \frac{i\omega}{f(z)} \left(z^2 \chi^2 - \frac{1}{z^2} \right) - \frac{1}{i\omega} \frac{m^2}{z^4} = 0, \quad (2.11)$$

and the IR boundary condition (2.7) and the UV relation (2.8) are changed into $\chi(z_h) = 1$ and $\eta_{\text{re}} = \chi_{\text{re}}(z_b)$, respectively.

⁴If $g_{tt}g_{rr} \neq 1$, this equation is still valid, but f and m^2 will represent the joint factors $\frac{1}{r^2} \sqrt{\frac{g_{tt}(r)}{g_{rr}(r)}}$ and $\sqrt{g_{tt}(r)g_{rr}(r)}m(r)^2$, respectively.

3 Machine learning algorithm

3.1 Neural ODE

In residual networks [46], there is a sequence of transformations to a hidden state

$$x_{t+1} = x_t + y_t(x_t, \theta_t), \quad (3.1)$$

where x_t is the hidden state at layer t , y_t is a differentiable function preserves the dimension of x_t , and θ_t denotes the transform parameters. The difference between x_{t+1} and x_t can be interpreted as a discretization of the derivative $x'(t)$ with the step $\Delta t = 1$. Adding more layers and decreasing the step, one can approach the limit

$$\frac{dx(t)}{dt} = y(x(t), t, \theta). \quad (3.2)$$

This equation can be used to represent the Neural ODE, an ODE induced by the continuous-depth limit of residual networks.

Given an initial state $x(t_0)$, the forward propagation of Neural ODEs yields the state $x(t_1)$ through a black-box ODE solver. The back propagation of Neural ODEs is realized by the adjoint sensitivity method [47]. Suppose that there is a loss function depending on the outputs of an ODE solver

$$L(x(t_1)) = L(x(t_0)) + \int_{t_0}^{t_1} y(x(t), t, \theta) dt. \quad (3.3)$$

The adjoint state is defined as

$$a(t) = \frac{\partial L}{\partial x(t)}. \quad (3.4)$$

It has been proven that the adjoint dynamics is dominated by another ODE

$$\frac{da(t)}{dt} = -a(t) \cdot \frac{\partial y}{\partial x}, \quad (3.5)$$

and the parameter gradient can be calculated by an integral [37]

$$\frac{\partial L}{\partial \theta} = \int_{t_1}^{t_0} a(t) \cdot \frac{\partial y}{\partial \theta} dt. \quad (3.6)$$

Now we can transform the flow equation into the Neural ODE. We first split the flow equation (2.11) into real and imaginary parts

$$\frac{d\chi_{\text{re}}}{dz} = \frac{2\omega z^2}{f} \chi_{\text{re}} \chi_{\text{im}}, \quad (3.7)$$

$$\frac{d\chi_{\text{im}}}{dz} = \frac{\omega}{f} \left[(z\chi_{\text{im}})^2 - (z\chi_{\text{re}})^2 + \frac{1}{z^2} \right] - \frac{m^2}{\omega z^4}. \quad (3.8)$$

Then we identify the shear response $(\chi_{\text{re}}, \chi_{\text{im}})$ with the state x and the radial coordinate z with the time t . In general, the function of metric $f(z)$ or the function of mass square $m^2(z)$ can be represented by a neural network with the parameter θ .

Obviously, given the parameter θ is equivalent to giving the trial function of metric or mass square which specifies the Neural ODE. By invoking an ODE solver, one can integrate from IR to UV and predict the real part of shear viscosity. Using the adjoint sensitivity method, one can implement back-propagation and perform training. We depict the architecture of the current algorithm in figure 1. Note that it differs from a typical Neural ODE in two aspects: the data is not a time series but only relates to the output at the upper limit of the integration, and one component of the adjoint state vanishes.

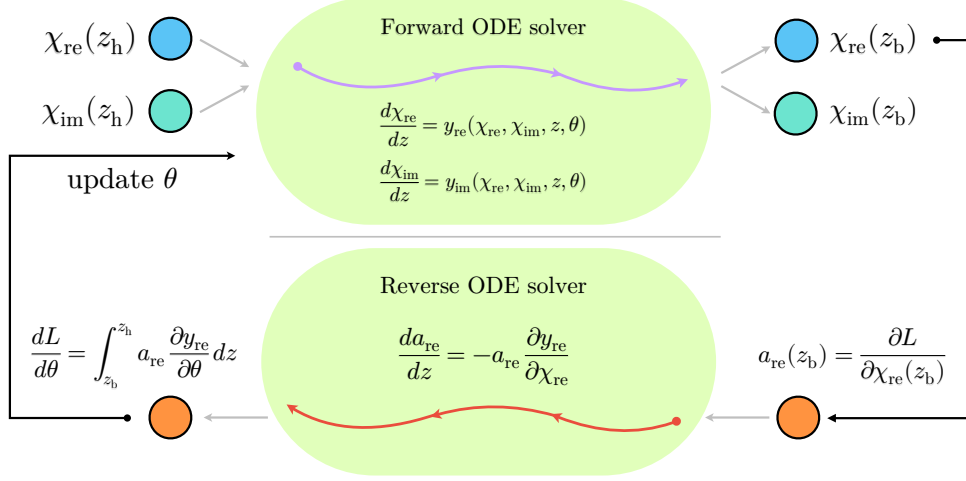


Figure 1: The architecture of the algorithm. The upper part depicts the forward propagation (from IR to UV) of the real and imaginary parts of the shear response. The lower part depicts the backward propagation of the adjoint state related only to the real part.

3.2 Loss function and inductive bias

Our loss function is chosen as the log-cosh form [48–51]

$$L = \frac{1}{N} \sum_{i=1}^N \log [\cosh (\eta_{\text{re}}(\omega_i, \theta) - \bar{\eta}_{\text{re}}(\omega_i))], \quad (3.9)$$

where N denotes the size of data, $\bar{\eta}_{\text{re}}$ represents the input data, and η_{re} is what the Neural ODE predicts. Note that the loss $\log [\cosh (x)]$ behaves like L1 loss $|x|$ far from the origin and L2 loss x^2 close to the origin. It is twice differentiable everywhere, making it suitable for optimizers like BFGS that require the Hessian [52].

We need to impose some inductive biases, which depend on different tasks.

Task 1: Learning the metric

Suppose that the graviton mass is given. Since we focus on finite temperature field theories, there should be a horizon at $z = 1$. This bias is implemented through the ansatz

$$f(z) = (1 - z)n_1(z, \theta_1), \quad (3.10)$$

where n_1 is a neural network with the trainable parameter θ_1 .

Task 2: Learning the mass

Suppose that the metric is given. We propose the ansatz

$$m(z)^2 = z^b n_2(z, \theta_2) \quad (3.11)$$

where the exponent b is a hyperparameter and n_2 is a neural network with the trainable parameter θ_2 . The purpose of separating z^b from $m(z)^2$ is to input the UV information $m(z)^2 \sim z^b + \dots$ through hyperparameter tuning, see Appendix B.

4 Holographic models

We will study three well-known holographic models without translation symmetry, all of which have homogeneous and isotropic backgrounds.

4.1 Massive gravity

The research of massive gravity (MG) has a long and winding history [53–57]. The main theoretical interest is to explore whether there exists a self-consistent theory that has a massive graviton with spin 2. In cosmology, MG is considered as a candidate theory that explains the accelerated expansion of the universe by modifying Einstein gravity. In holography, massive gravity is the first analytically tractable model without translation symmetry [58]

We will consider the dRGT massive gravity that is claimed to be ghost free [59–61]. Its simplest version used in holography is described by the bulk action

$$S_{\text{bulk}} = \int d^4x \sqrt{-g} (\mathcal{R} + 6 - \alpha \text{tr} \mathcal{X}), \quad (4.1)$$

where $\mathcal{X}^\mu{}_\nu = \sqrt{g^{\mu\lambda} f_{\lambda\nu}}$ and $f_{\mu\nu} = \text{diag}(0, 0, 1, 1)$ is the reference metric. Note that we have set the AdS radius to one for convenience.

Using the action, one can derive the Einstein equation

$$R_{\mu\nu} - \frac{1}{2} g_{\mu\nu} R - 3g_{\mu\nu} = \frac{1}{2} \alpha (\mathcal{X}_{\mu\nu} - g_{\mu\nu} \text{tr} \mathcal{X}). \quad (4.2)$$

This allows for the existence of a black hole solution (2.10) with the emblackening factor

$$f(z) = 1 - z^3 - \frac{\alpha}{2} z(1 - z^2). \quad (4.3)$$

The black hole is associated with the Hawking temperature

$$T = \frac{1}{4\pi} (3 - \alpha), \quad (4.4)$$

which should be non-negative. Inserting the energy-momentum tensor

$$T_{\mu\nu} = \alpha (\mathcal{X}_{\mu\nu} - g_{\mu\nu} \text{tr} \mathcal{X}) \quad (4.5)$$

into eq. (2.4), one can calculate the square of graviton mass

$$m^2 = \frac{\alpha}{2} z. \quad (4.6)$$

Now we can generate the data for training. Inputting eq. (4.3) and eq. (4.6) into eq. (2.11), using the regular condition at the horizon, and setting the parameter $\alpha = 1$, one can solve the flow equation and obtain the real part of shear viscosity on the boundary. We sample the frequency uniformly between 0.01 and 6 to generate 600 data points $[\omega, \eta_{\text{re}}(\omega)]$, which are plotted in the left panel of figure 2.

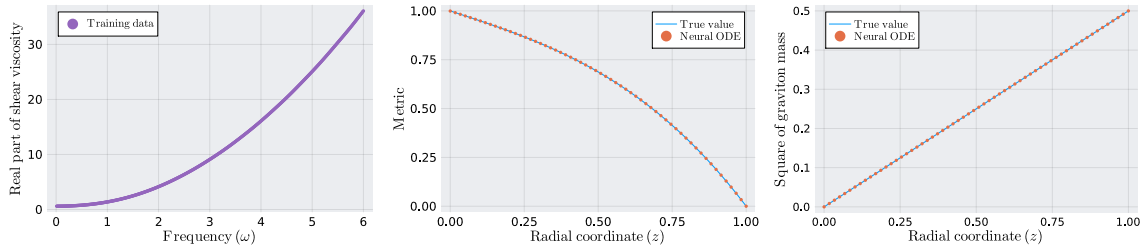


Figure 2: Training data and performance of Neural ODEs for the MG model. The left panel shows the real part of the frequency-dependent shear viscosity, obtained by solving the flow equation with the true metric and mass. The middle and right panels illustrate the performance of Neural ODEs in learning the metric and mass respectively, where the curves represent the true values and the dots indicate the predictions.

We conduct two numerical experiments: fixing the mass to learn the metric and fixing the metric to learn the mass. The primary training results are shown in the middle and right panels of figure 2. Additionally, figure 6 and table 1 in Appendix B detail the hyperparameter tuning, minimum loss, and mean relative error (MRE).

4.2 Linear axions

The simplest holographic mechanism for breaking translation symmetry is to invoke the linear axion (LA) [62]. Consider the Einstein gravity minimally coupled with two massless scalar fields. Its bulk action is given by

$$S_{\text{bulk}} = \int d^4x \sqrt{-g} (\mathcal{R} + 6 - X), \quad (4.7)$$

where $X = g^{\mu\nu} X_{\mu\nu}$ and $X_{\mu\nu} = G_{IJ} \partial_\mu \chi^I \partial_\nu \chi^J$ with $G_{IJ} = \frac{1}{2} \text{diag}(1, 1)$ and $I = 1, 2$.

The equations of motion following the action are

$$R_{\mu\nu} - \frac{1}{2} g_{\mu\nu} R - 3g_{\mu\nu} = X_{\mu\nu} - \frac{1}{2} g_{\mu\nu} X, \quad (4.8)$$

$$\nabla^2 \chi^I = 0. \quad (4.9)$$

They admit a black hole solution

$$f(z) = 1 - z^3 + \frac{\beta^2}{2} z^2 (z - 1) \quad (4.10)$$

with the temperature

$$T = \frac{1}{8\pi} (6 - \beta^2), \quad (4.11)$$

when the axions are linear

$$\chi^1 = \beta x, \chi^2 = \beta y. \quad (4.12)$$

Using the energy-momentum tensor

$$T_{\mu\nu} = 2X_{,\mu\nu} - g_{\mu\nu}X \quad (4.13)$$

and eq. (2.4), we read the square of graviton mass

$$m^2 = \beta^2 z^2. \quad (4.14)$$

With eq. (4.10) and eq. (4.14) in hand, we can generate the data. Here we fix the parameter $\beta = 1$. Other setting is similar to before. The data $[\omega, \eta_{\text{re}}(\omega)]$ are plotted in the left panel of figure 3. The training results are displayed in the middle and right panels of figure 3, as well as in figure 6 and table 1.

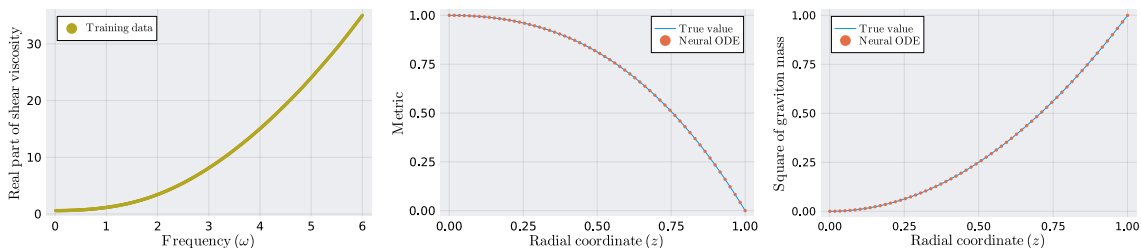


Figure 3: Training data and performance of Neural ODEs for the LA model. Left panel: the real part of the frequency-dependent shear viscosity. Middle and right panels: The performance of Neural ODEs in learning the metric and mass.

4.3 Generalized axions

In the above two models with broken translation symmetry, the mass square of the graviton has only one term. One may wonder if Neural ODEs can learn more general mass function. Here we will study the generalized axion (GA) model [63], which is a productive tool in the field of holographic condensed matters [64], see a recent application in amorphous solids [65]. Of particular interest to us, it can assign more general mass function to the graviton, while remaining analytically tractable.

Let's generalize the bulk action (4.7) to the form

$$S_{\text{bulk}} = \int d^4x \sqrt{-g} (\mathcal{R} + 6 - V(X)). \quad (4.15)$$

We will select the function $V(X)$ that has been used in [63]

$$V(X) = \gamma_1 X + \gamma_5 X^5, \quad (4.16)$$

where γ_1 and γ_5 are two parameters.

Taking the variation of the action, we can write down the equations of motion

$$R_{\mu\nu} - \frac{1}{2}g_{\mu\nu}R - 3g_{\mu\nu} = X_{\mu\nu}V'(X) - \frac{1}{2}g_{\mu\nu}V(X), \quad (4.17)$$

$$\nabla_\mu V' \nabla^\mu \chi^I + V' \nabla^2 \chi^I = 0. \quad (4.18)$$

They have the analytical solution

$$f(z) = 1 - z^3 + \frac{1}{2} \sum_{n=1,5} \gamma_n \frac{z^3 - z^{2n}}{3 - 2n},$$

$$\chi^1 = x, \quad \chi^2 = y. \quad (4.19)$$

From the metric, we can read the temperature

$$T = \frac{1}{8\pi} \left(6 - \sum_{n=1,5} \gamma_n \right). \quad (4.20)$$

We can also derive the graviton mass from eq. (2.4) and

$$T_{\mu\nu} = 2X_{\mu\nu}V'(X) - g_{\mu\nu}V(X), \quad (4.21)$$

which yields

$$m^2 = \sum_{n=1,5} n\gamma_n z^{2n}. \quad (4.22)$$

Using eq. (4.19) and eq. (4.22), the data are generated in the left panel of figure 4. Here we have fixed the parameters $\gamma_1 = \gamma_5 = 1$. We exhibit the training results in middle and right panels of figure 4, as well as in figure 6 and table 1.

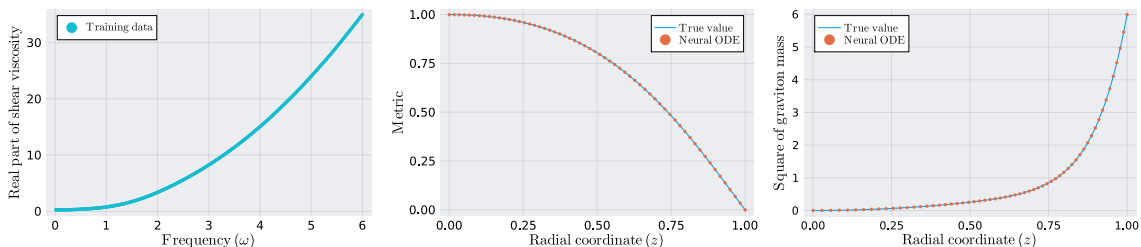


Figure 4: Training data and performance of Neural ODEs for the GA model.

5 Conclusion and discussion

This work introduces an important physical ingredient to AdS/DL: translation symmetry breaking. Specifically, we extend the data-driven holographic transport model proposed in [32], allowing the machine to learn the black hole metric or the graviton mass from the real part of the shear viscosity⁵. In addition, we use the Neural ODE to learn continuous

⁵In [32], the model is subject to the several constraints: minimal coupling of 3+1 dimensional Einstein gravity and matter, homogeneous and isotropic background, vanishing graviton mass, and the relation $\eta = \chi + i\omega r$ on the boundary. In the current work, we allow for a non-zero graviton mass and reduce the boundary relation to its real part.

functions, thereby avoiding the problem of discretization errors. Around these physical and technical results, we have made the following comments and explorations.

1) Universality of theoretical framework

Although some assumptions still remain, the current theoretical framework, which mainly consists of the wave equation (2.3), the regularity at the horizon (2.7), and the boundary relation (2.8), is very general. Considering that the holographic calculation of shear viscosity does not impose the probe limit, this generality is quite rare and precious.

2) Reconstruction of graviton mass

There are many ways to reconstruct the function of metric, but there has been no way to reconstruct the function of graviton mass before. Our work fills this gap, which may help to better understand the gravity dual of translation symmetry breaking in bottom-up holographic models.

3) At low temperatures

In Table 1, it is shown that the Neural ODE can achieve high accuracy for the bulk reconstruction. However, we caution that this is associated with the current model parameters (α, β, γ) , which are simply fixed to 1. As these parameters increase, the temperature of black holes decreases. Meanwhile, we observe a rapid degradation in the performance of Neural ODEs⁶. To address this issue, we will specify the temperature by hyperparameter tuning and input several inductive biases. In this way, Neural ODEs can still perform well, see Appendix C.

4) Entanglement entropy

In [29], after the bulk metric is learned from lattice QCD data, the quark-antiquark potential is calculated using the holographic method. Interestingly, this potential exhibits both a linear confining part and a Debye screening part. In Appendix D, we conduct a similar exploration.

Using the bulk metric $f(z)$ learned from the shear viscosity $\eta_{\text{re}}(\omega)$, we calculate the derivative $S'(l)$, where S is the holographic EE and l is the spatial size of entangling region⁷. Across a wide range of l spanning several orders of magnitude, we find that the MRE of $S'(l)$ is very small. This indicates that we have established a relationship between $S'(l)$ and $\eta_{\text{re}}(\omega)$. Note that this relationship may be very complex from the perspective of field theories, partly because $S'(l)$ and $\eta_{\text{re}}(\omega)$ belong to two distinct classes of observables: quantum information measures and transport coefficients. Nevertheless, using the bulk metric as a medium, $S'(l)$ and $\eta_{\text{re}}(\omega)$ can indeed be linked via the Neural ODE and the Ryu-Takayanagi (RT) formula [66], see figure 5.

More importantly, the relationship between $S'(l)$ and $\eta_{\text{re}}(\omega)$ is independent with the probe limit and is not confined to a specific model⁸. Based on its generality and robustness⁹,

⁶Similar phenomena were previously reported in [33].

⁷We focus on the derivative of EE rather than the EE itself because the former is not sensitive to the UV cutoff [23–25].

⁸For any effective methods of bulk metric reconstruction, their field-theory observables are interrelated, reflecting at least a redundancy in the bulk geometry information. However, each reconstruction method has its applicable range. If these ranges are very limited or only slightly overlap, we would not expect a clear relationship between the field-theory observables.

⁹It is found that the relative error of $S'(l)$ decreases oscillatingly as l increases, indicating a more robust

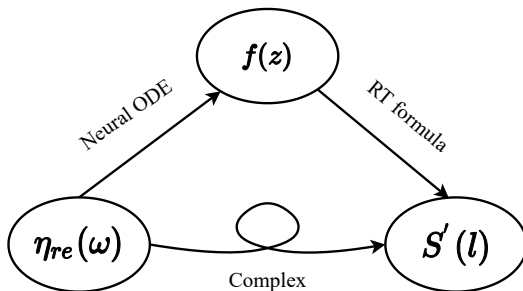


Figure 5: The schematic diagram for the relationship between $\eta_{re}(\omega)$ and $S'(l)$. At the bulk level, they are connected by the Neural ODE and the RT formula through the metric, which is represented by the straight arrows above. The curved arrow below indicates that the relationship between them can be very complicated from the perspective of field theory.

we conjecture that this relationship may manifest in some real-world strongly coupled systems. In particular, given the recent progress in lattice gauge theories with respect to both $S'(l)$ and the spectral function related to shear viscosity [24, 67, 68], we expect that this conjecture could be verified in the near future.

5) Beyond AdS/CFT

The current theoretical framework necessitates that the bulk spacetime be asymptotically AdS. However, we deliberately refrain from explicitly communicating this information to the machine. Our intentional omission increases the training difficulty considerably, but the performance of Neural ODEs remains excellent. This encouraging result suggests the potential to develop a machine-learning framework that extends beyond asymptotic AdS, encompassing the Lifshitz and hyperscaling-violated geometries, as well as other novel behaviors¹⁰.

Ultimately, this work falls within the realm of reverse engineering of AdS/CFT, where the holographic dictionary is given a priori. One can also develop holographic machine learning that is independent of AdS/CFT [69–72], which explores the emergence of spacetime and gravity from a more fundamental level.

Acknowledgments

We thank Xian-Hui Ge, Yan Liu, Zhen-Kang Lu, Yu Tian, and Zhuo-Yu Xian for helpful discussions. SFW was supported by NSFC grants (No.11675097, No.12275166, and No.12311540141).

relationship in the IR. This robustness could facilitate the emergence of the relationship in the real-world strongly coupled systems that lack conformal symmetry in the UV.

¹⁰By constructing a free bulk theory from the generalized free fields on the boundary, it was found recently that the Sachdev-Ye-Kitaev model retains geometric bulk features beyond its conformal limit [26]. Notably, the curvature of the emergent spacetime diverges near the boundary.

A From shear response to shear viscosity

Consider the bulk action of the Einstein gravity minimally coupled with the matter

$$S_{\text{bulk}} = \int d^4x \sqrt{-g} (R + 6 + L_{\text{matter}}), \quad (\text{A.1})$$

and the wave equation of the shear mode

$$\frac{1}{\sqrt{-g}} \partial_r (\sqrt{-g} g^{rr} \partial_r h) + (\omega^2 g^{tt} - m^2) h = 0. \quad (\text{A.2})$$

We require that the metric and graviton mass can be expanded near the AdS boundary, with the form

$$\begin{aligned} g_{tt} &= r^2 \left(1 + \frac{a_1}{r} + \frac{a_2}{r^2} + \frac{a_3}{r^3} + \dots \right), \\ g^{rr} &= r^2 \left(1 + \frac{b_1}{r} + \frac{b_2}{r^2} + \frac{b_3}{r^3} + \dots \right), \\ m^2 &= r^{-v} \left(c_0 + \frac{c_1}{r} + \frac{c_2}{r^2} + \frac{c_3}{r^3} + \dots \right), \end{aligned} \quad (\text{A.3})$$

where (a_i, b_i, c_i) are some constants and v is a positive integer.

Inserting eq. (A.3) into eq. (A.2), one can find that the asymptotic solution of the wave equation can be written as

$$h = h^{(0)} \left(1 + d_1 \frac{1}{r^1} + d_2 \frac{1}{r^2} + d_3 \frac{\log(r)}{r^3} \right) + h^{(3)} \frac{1}{r^3} + \dots \quad (\text{A.4})$$

Here $h^{(0)}$ is the source, $h^{(3)}$ depends on $h^{(0)}$ and the incoming boundary condition on the horizon, and d_i is determined by the frequency and the constants a_i, b_i, c_i and v .

To ensure a well-defined variational system, we need the Gibbons-Hawking term and the counterterms

$$S_{\text{GH}} = 2 \int d^3x \sqrt{-\gamma} K, \quad S_{\text{ct}} = \int d^3x \sqrt{-\gamma} \left(-4 - R + L_{\text{matter}}^{(1)} \right), \quad (\text{A.5})$$

where $L_{\text{matter}}^{(1)}$ denotes the contribution of the counterterms from the matter. We will expand the on-shell bulk action, the Gibbons-Hawking term, and the counterterms to the second order of the shear mode. Here the key step is to calculate the second-order variation of the matter action $S_{\text{m}} = \int d^4x \sqrt{-g} L_{\text{matter}}$ as follows:

$$\begin{aligned} \frac{\delta^2 S_{\text{m}}}{\delta g_{xy}^2} &= \frac{1}{2} \left[\frac{\delta S_{\text{m}}}{\delta g^{xx}} \frac{\delta^2 g^{xx}}{(\delta g_{xy})^2} + \frac{\delta^2 S_{\text{m}}}{(\delta g^{xx})^2} \left(\frac{\delta g^{xx}}{\delta g_{xy}} \right)^2 + x \leftrightarrow y \right] \\ &+ \frac{1}{2} \left[\frac{\delta S_{\text{m}}}{\delta g^{xy}} \frac{\delta^2 g^{xy}}{(\delta g_{xy})^2} + \frac{\delta^2 S_{\text{m}}}{(\delta g^{xy})^2} \left(\frac{\delta g^{xy}}{\delta g_{xy}} \right)^2 + x \leftrightarrow y \right]. \end{aligned} \quad (\text{A.6})$$

Since $T_{\mu\nu} = -2 \frac{1}{\sqrt{-g}} \frac{\delta S_{\text{m}}}{\delta g^{\mu\nu}}$ and

$$g^{xx} = g^{yy} = \frac{g_{xx}}{-g_{xy}^2 + g_{xx}^2}, \quad g^{xy} = \frac{-g_{xy}}{-g_{xy}^2 + g_{xx}^2}, \quad (\text{A.7})$$

one can read

$$\frac{\delta^2 S_m}{\delta g_{xy}^2} = -\frac{\sqrt{-g}}{g_{xx}^2} \left(\frac{1}{g_{xx}} T_{xx} - \frac{1}{2} \frac{\delta T_{xy}}{\delta g_{xy}} \right). \quad (\text{A.8})$$

Using eq. (A.8) and the Einstein equation for the background metric

$$\frac{1}{2} T_{xx} = -3g_{xx} - \frac{g_{xx} g'_{rr} g'_{tt}}{4g_{rr}^2 g_{tt}} - \frac{g_{xx} g_{tt}^2}{4g_{rr} g_{tt}^2} - \frac{g'_{rr} g'_{xx}}{4g_{rr}^2} + \frac{g'_{tt} g'_{xx}}{4g_{rr} g_{tt}} - \frac{g_{xx}^2}{4g_{rr} g_{xx}} + \frac{g_{xx} g_{tt}''}{2g_{rr} g_{tt}} + \frac{g_{xx}''}{2g_{rr}}, \quad (\text{A.9})$$

we can perform the expansion and express the result in the frequency space

$$S_{\text{bulk}} + S_{\text{GH}} + S_{\text{ct}}|_{\text{on-shell}} = \int d^2x \int_{-\infty}^{\infty} \frac{d\omega}{2\pi} \frac{1}{2} \left[\left(L_{\text{gravity}}^{(2)} + L_{\text{matter}}^{(2)} \right) \bar{h}h - g_{xx} \sqrt{\frac{g_{tt}}{g_{rr}}} \bar{h}h' \right], \quad (\text{A.10})$$

where \bar{h} has the argument $-\omega$. In the terms $\sim \bar{h}h$, $L_{\text{gravity}}^{(2)}$ can be referred as the gravity contribution and $L_{\text{matter}}^{(2)}$ denotes the contribution from $L_{\text{matter}}^{(1)}$. One can find that $L_{\text{gravity}}^{(2)}$ has the form

$$L_{\text{gravity}}^{(2)} = -\omega^2 \frac{g_{xx}}{\sqrt{g_{tt}}} + 4\sqrt{g_{tt}g_{xx}} - \frac{g_{xx}g'_{tt}}{\sqrt{g_{tt}g_{rr}}} - \sqrt{\frac{g_{tt}}{g_{rr}}} g'_{xx}. \quad (\text{A.11})$$

Interestingly, it is independent with the energy-momentum tensor and the graviton mass. In contrast, we can not write down the general form of $L_{\text{matter}}^{(2)}$.

One may notice that $L_{\text{gravity}}^{(2)}$ and $L_{\text{matter}}^{(2)}$ usually diverge at the boundary. To deal with the divergence, we input eq. (A.3) and eq. (A.4) into eq. (A.10), which yields the renormalized action

$$S_{\text{ren}} = \int d^2x \int_{-\infty}^{\infty} \frac{d\omega}{2\pi} \frac{1}{2} \left[\left(L_{\text{gravity}}^{(3)} + L_{\text{matter}}^{(3)} \right) \bar{h}^{(0)}h^{(0)} + 3\bar{h}^{(0)}h^{(3)} \right], \quad (\text{A.12})$$

where $L_{\text{gravity}}^{(3)}$ and $L_{\text{matter}}^{(3)}$ are finite and they are contributed by the gravity and the matter, respectively. In terms of eq. (A.11), it is obvious that $L_{\text{gravity}}^{(3)}$ is real since it is composed of the real constants in eq. (A.3). Moreover, we will assume that $L_{\text{matter}}^{(3)}$ is also real. This assumption is valid for all holographic models in the main text. To prove this, we will list their counterterms explicitly.

1) Massive gravity

The counterterms of massive gravity have been derived in [73]. They can be expressed as

$$S_{\text{ct}} = \int d^3x \sqrt{-\gamma} \left[-4 - R + \frac{1}{2} \alpha e_1 + \frac{1}{16} \alpha^2 e_2 + \frac{\alpha}{4} (2R_{ij} Y^{ij} - e_1 R) \log r \right], \quad (\text{A.13})$$

from which we calculate

$$L_{\text{matter}}^{(2)} = -\frac{1}{8} \alpha \left(\sqrt{g_{tt}g_{xx}} + 2\omega^2 \sqrt{\frac{g_{xx}}{g_{tt}}} \log r \right). \quad (\text{A.14})$$

2) Linear axions

The counterterms of the linear axion model are simple:

$$S_{\text{ct}} = \int d^3x \sqrt{-\gamma} (-4 - R + \gamma^{ij} X_{ij}). \quad (\text{A.15})$$

We can read

$$L_{\text{matter}}^{(2)} = -\frac{1}{2}\beta^2 \sqrt{g_{tt}}. \quad (\text{A.16})$$

3) Generalized axions

In terms of the holographic renormalization studied in [74], one can infer that the counterterms of generalized axion model are given by

$$S_{\text{ct}} = \int d^3x \sqrt{-\gamma} (-4 - R + \gamma_1 \gamma^{ij} X_{ij}), \quad (\text{A.17})$$

which indicates

$$L_{\text{matter}}^{(2)} = -\frac{1}{2}\gamma_1 \sqrt{g_{tt}}. \quad (\text{A.18})$$

From eq. (A.14), eq. (A.16), and eq. (A.18), it is obvious that they can only generate real $L_{\text{matter}}^{(3)}$.

Motivated by these explicit examples, let's move on a more general analysis. Suppose that a counterterm is an intrinsic scalar on the boundary, which consists of the induced metric, matter fields, and their derivatives. To be safe, we will focus on neutral matter fields and impose the parity symmetry¹¹. One can see that $L_{\text{matter}}^{(3)}$ cannot have an imaginary part unless the expansion of $L_{\text{matter}}^{(1)}$ contains a term

$$L_{\text{im}} \sim \gamma^{tt} \partial_t \gamma_{xy} \gamma_{xy} (\Psi, \partial\Psi)_{t\dots}, \quad (\text{A.19})$$

where $(\Psi, \partial\Psi)_{t\dots}$ denotes certain matter field or its spatial derivative with the indices $t\dots$. The expression of L_{im} is understood that the subscript t in $\partial_t \gamma_{xy}$ must be paired with the subscript t in $(\Psi, \partial\Psi)_{t\dots}$ in order to contract with the superscripts of g^{tt} . Obviously, Ψ is neither a scalar nor a spinor since they have no spacetime indices. Ψ is also not a U(1) vector: Due to the gauge symmetry, the U(1) vector can only appear in the form of $F_{ij} F^{ij}$, which cannot be paired with $\partial_t \gamma_{xy}$. In light of these analysis, one can find that our assumption is valid for all Einstein-Maxwell-Dirac-scalar models with parity symmetry and neutral matters. For more general models, we cannot provide a similar proof by checking eq. (A.19). Nevertheless, keeping in mind the intrinsic structure of counterterms¹², it is reasonable to suspect that the current assumption may be valid in a more general situation¹³. In fact, we are not aware of any obvious counterexamples.

To proceed, we consider a field theory lived in a two-dimensional flat space and define the retarded correlator[32, 76]

$$G_{T_{xy}T_{xy}}^R(t) \equiv \frac{4\delta^2 W}{\delta h_{axy}(t) \delta h_{rxy}(0)}, \quad (\text{A.20})$$

¹¹Then the Levi-Civita tensor can be excluded in building the counterterm.

¹²Even if one can construct a counterterm ansatz that yields L_{im} , this does not necessarily imply that it is a genuine counterterm for a specific model. In [74], it was found that the exact ansatz of counterterms can be generated from the radial Hamiltonian, indicating the existence of an intrinsic structure of counterterms.

¹³For example, consider the famous model of holographic superconductor [?]. The charged complex scalar field Φ is coupled with the U(1) vector A , which in principle might produce: $L_{\text{im}} \sim \gamma^{tt} \partial_t \gamma_{xy} \gamma_{xy} |(\partial_t - iA_t)\Phi|$. However, the matter contribution to the counterterm of this model is just $L_{\text{matter}}^{(1)} \sim |\Phi|^2$.

where W is the generating functional, δh_{xy} denotes the shear perturbation of the metric, and the subscripts (r, a) indicate the closed time-path formalism.

Using the holographic dictionary, one can read the retarded correlator from eq. (A.12):

$$G_{T^{xy}T^{xy}}^R(\omega) = L^{(3)} + 3\frac{h^{(3)}}{h^{(0)}}, \quad (\text{A.21})$$

where $L^{(3)} = L_{\text{gravity}}^{(3)} + L_{\text{matter}}^{(3)}$. Expand the response function near the boundary, which yields

$$\chi(\omega)|_{r \rightarrow \infty} = \frac{\Pi}{i\omega h} \Big|_{r \rightarrow \infty} = -\frac{\sqrt{-g}g^{rr}\partial_r h}{i\omega h} \Big|_{r \rightarrow \infty} = \frac{1}{i\omega} \left(\frac{3h^{(3)}}{h^{(0)}} - e_1 \right) \Big|_{r \rightarrow \infty}. \quad (\text{A.22})$$

Here e_1 is real, relying on r , ω , and previous constants. Comparing eq. (A.21) and eq. (A.22), we have

$$\chi(\omega)|_{r \rightarrow \infty} = \frac{1}{i\omega} G_{T^{xy}T^{xy}}^R(\omega) - \frac{1}{i\omega} \left(L^{(3)} + e_1 \right) \Big|_{r \rightarrow \infty}. \quad (\text{A.23})$$

Importantly, the last term of eq. (A.23), which depends on the UV details of specific models, is purely imaginary.

In view of this, we will consider the Kubo formula for the real part of the frequency-dependent shear viscosity [32, 41, 76]

$$\eta_{\text{re}}(\omega) = \frac{1}{\omega} \text{Im} [G_{T^{xy}T^{xy}}^R(\omega)]. \quad (\text{A.24})$$

Combining eq. (A.23) and eq. (A.24), we finally obtain a simple equality between the shear viscosity and the shear response

$$\eta_{\text{re}}(\omega) = \chi_{\text{re}}(\omega)|_{r \rightarrow \infty}. \quad (\text{A.25})$$

B Training scheme and report

In order to perform training, we need to make some settings.

1) Neural network

We use a neural network to represent the metric or mass. It is a fully connected feed-forward network consisting of three dense layers:

$$(1, 5) \rightarrow (5, 5, \tanh) \rightarrow (5, 1). \quad (\text{A.1})$$

For each layer, we have specified the number of input nodes and output nodes. In the second layer, a tanh activation is used. Note that the neural network has 46 trainable parameters, which include weights and biases.

2) ODE solver

Our Neural ODEs are solved using the Tsitouras 5/4 method [77], which is an adaptive and explicit Runge-Kutta method.

3) IR and UV cutoffs

In solving the ODEs numerically, the horizon and boundary cannot be touched exactly. We set the IR and UV cutoffs as $z_{\text{IR}} = 0.9999$ and $z_{\text{UV}} = 0.0001$.

4) Initial values

To learn the metric, the neural network is initialized by sampling from a standard normal distribution $\mathcal{N}(0, 1)$. The normal distribution $\mathcal{N}(0, 0.001)$ with a small standard deviation is utilized for learning the mass and hyperparameter tuning.

5) Hyperparameter tuning

There are various hyperparameter tuning methods, which consume different computing resources. Here we propose a simple way to quickly find the exponent b in the square of graviton mass. We define the search range as $[0, 4]$ with the step size 1. We use the standard cross-validation method with the simple hold-out technique [78]. We separate the dataset within the frequency range $[0.01, \omega_{\text{max}}]$ into two parts. The part with $[0.01, \omega_{\text{max}} - 1]$ goes to the training set and the part with $[\omega_{\text{max}} - 0.99, \omega_{\text{max}}]$ to the validation set. The rationale for this separation lies in the dependence of the exponent b on the UV physics. We use the optimizers RMSProp and Adam in order. Their learning rates, epoch numbers, and batch sizes are set as $(0.001, 0.0001)$, $(10, 10)$ and $(1, 1)$. We also add the L1 regularization term $L_1 = 0.1 \times |\theta|$ in the loss function. For each b in the search range, we train 5 times and take the average validation error to select the optimal b . As long as ω_{max} is large enough, the correct b can be found for the current three targets. Specifically, $\omega_{\text{max}} = 2$ is large enough for the MG and LA models, and $\omega_{\text{max}} = 4$ is large enough for the GA model, see figure 6.

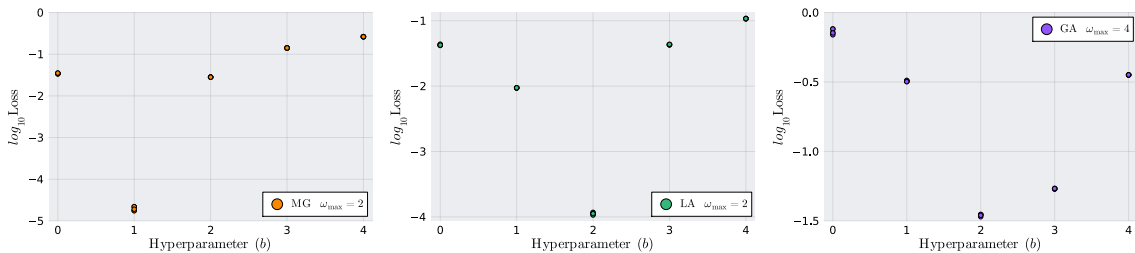


Figure 6: The hyperparameter tuning of b in the MG (left), LA (middle) and GA (right) models. Each b is trained five times, yielding five nearly coincident loss function points in most cases. As one can see, the optimal hyperparameters for three models are 1, 2, and 2, respectively.

It should be noted that our hyperparameter tuning method has its limitations. Considering the true mass square with the UV behavior $m^2 = az^b + \dots$, we observe that the required ω_{max} increase as a decreases. However, even if b cannot be found accurately, the final learned curve of the mass square usually deviates only slightly at UV. In the future, more sophisticated hyperparameter tuning methods can be explored to improve the results, if necessary.

6) Training process

The training process can be divided into multiple stages, which are described as follows.

a) In most cases, the optimizers (RMSProp, Adam, Adam, BFGS) are used sequentially in four stages. For learning the mass of the MG and the LA models, only the first two

training stages are needed, as the log-cosh loss becomes negligible (less than the machine epsilon $\sim 1 \times 10^{-16}$).

b) The learning rates (0.001, 0.0001, 0.00001) are used sequentially in first three stages. The epoch numbers are (10, 10, 100) respectively. The batch sizes are all set as 1. In the fourth stage, the initial size of the step is set as 0.01 and the maximum number of iterations is set as 500.

c) In the first stage, we train $N_1 = 120$ times, each time with randomly initialized trainable parameters. In the i -th stage with $i > 1$, we obtain the initial parameters from the top $N_i = N_{i-1}/2$ trained results with the minimum loss in the $(i-1)$ -th stage. We conduct parallel training on multiple computer cores. When more than $N_i/2$ tasks are completed, we stop the i -th stage and move on to the $(i+1)$ -th stage. This early stopping can effectively prevent the machine from getting stuck in solving Neural ODEs with bad parameters.

After training, we collect information on the best result, including the minimum loss, the MRE of the learned metric, and the MRE of the learned mass square, see table 1. Note that the MRE is calculated by uniformly sampling 100 points within the allowed range of the radial coordinate z .

Target	f of MG	m^2 of MG	f of LA	m^2 of LA	f of GA	m^2 of GA
Loss	7×10^{-10}	$< 1 \times 10^{-16}$	2×10^{-10}	$< 1 \times 10^{-16}$	6×10^{-10}	1×10^{-11}
MRE	5×10^{-5}	3×10^{-9}	1×10^{-5}	2×10^{-10}	7×10^{-5}	6×10^{-4}

Table 1: Minimum loss and MRE of six machine learning experiments. Their learning targets are the metric and mass square in the models of MG, LA and GA.

C At low temperatures

In order to learn the low-temperature physics, we will modify the algorithm as follows.

1) Loss function

We will use a new loss function

$$L = \frac{1}{N} \sum_{i=1}^N \frac{1}{2} \left[\left| \frac{\eta_{\text{re}}(\omega_i, \theta)}{\bar{\eta}_{\text{re}}(\omega_i)} \right| - 1 - \log \left| \frac{\eta_{\text{re}}(\omega_i, \theta)}{\bar{\eta}_{\text{re}}(\omega_i)} \right| \right], \quad (\text{A.1})$$

which is a combination of relative error and logarithmic difference. It has a natural physical origin and will be elaborated in [79]. Here we introduce it just by experience.

2) Ansatz

We change the previous metric ansatz as

$$f = (1 - z)[4\pi T + (1 - z)n_1(z, \theta_1)], \quad (\text{A.2})$$

where the temperature T will be specified by hyperparameter tuning. Note that this scheme reduces the difficulty of learning near-horizon geometry.

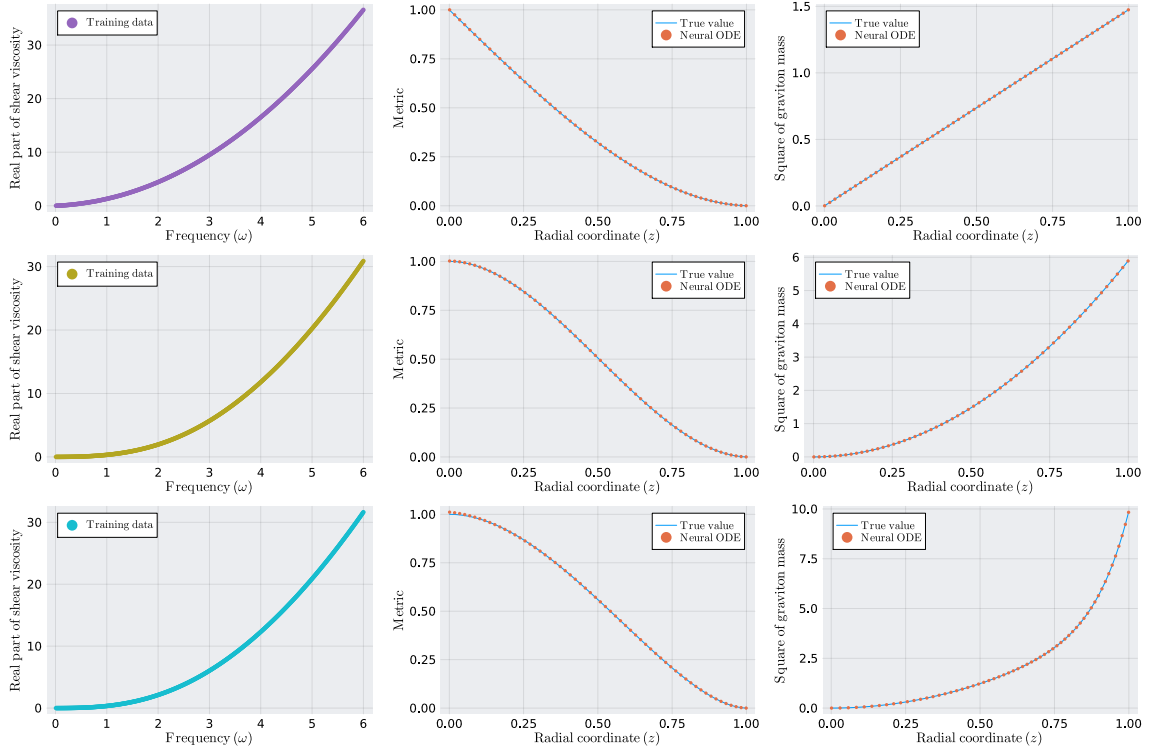


Figure 7: Training data and performance of Neural ODEs for the MG (top), LA (middle) and GA (bottom) model at low temperatures.

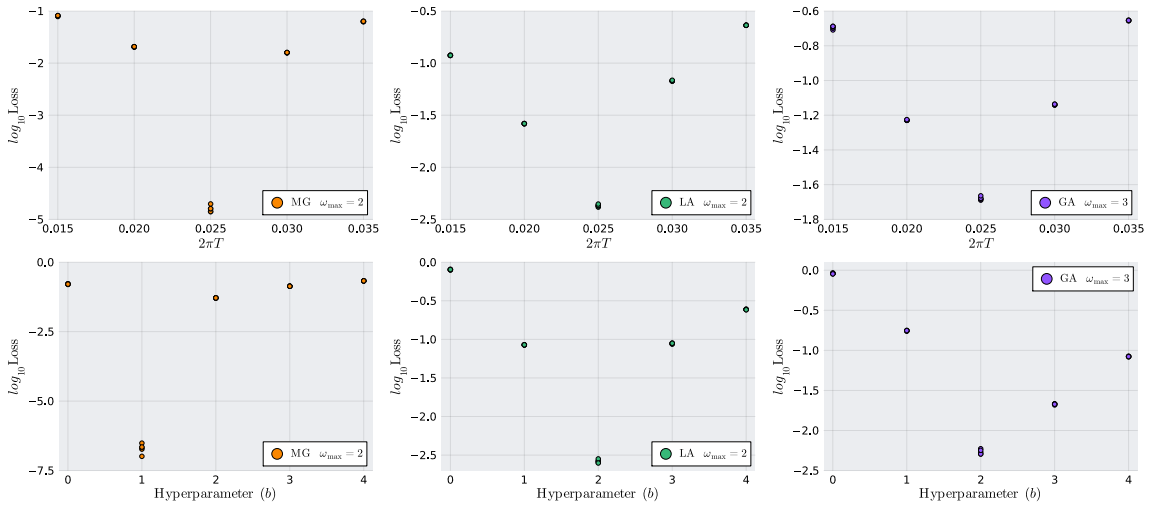


Figure 8: The hyperparameter turning of $2\pi T$ (top) and b (bottom) in three models at low temperatures.

We also change the previous mass ansatz as

$$m^2 = z^b e^{n_2(z, \theta_2)}. \quad (\text{A.3})$$

This is beneficial for learning the mass square in the GA model at low temperatures, where

m^2/z^2 grows fast near the horizon. Note that for the low-temperature MG and LA models, as well as all the relatively high-temperature models studied in the main text, the ansatz (A.3) remains applicable, and the performance of Neural ODEs will not be significantly affected. The only price of using (A.3) is to assume that the mass square is positive¹⁴.

3) ODE solver

Since the Tsitouras 5/4 is less stable at low temperatures, we change the solver to the Radau IIA5 [80], which is a fully implicit Runge-Kutta method and has high numerical stability.

4) Cutoffs

We set the IR and UV cutoffs as $z_{\text{IR}} = 0.999$ and $z_{\text{UV}} = 0.001$, by which the low-temperature data can still be generated with sufficient accuracy.

5) Initial values

When learning the mass square of MG and LA models and tuning the hyperparameters T and b , we initialize the neural network with the normal distribution $\mathcal{N}(0, 0.001)$. For other tasks, we use $\mathcal{N}(0, 1)$.

6) Hyperparameter tuning

The method of tuning b remains the same as before. For tuning T , the main difference is in the dataset separation: we randomly shuffle the dataset within the frequency range $[0.01, \omega_{\text{max}}]$ and split it into two parts: 70% for the training set and 30% for the validation set. Additionally, we remove the L1 regularization.

In figures 7-8 and table 2, we generate the data and illustrate the performance of Neural ODEs at low temperatures. We choose the parameters ($2\alpha = 5.9$, $\beta^2 = 5.9$, $\gamma_1 = 4.9$, $\gamma_5 = 1$), which correspond to the same temperature $T \simeq 0.004$.

Target	f of MG	m^2 of MG	f of LA	m^2 of LA	f of GA	m^2 of GA
Loss	3×10^{-7}	$< 1 \times 10^{-16}$	3×10^{-10}	$< 1 \times 10^{-16}$	9×10^{-8}	2×10^{-8}
MRE	1×10^{-3}	8×10^{-10}	2×10^{-4}	2×10^{-9}	1×10^{-3}	1×10^{-4}

Table 2: Minimum loss and MRE of six machine learning experiments at low temperatures.

D Entanglement entropy

At last, we will use the bulk metric learned by Neural ODEs to predict the derivative of EE with respect to the size of entangling region.

Consider the region A to be a spatial strip with infinite length L and width l on the boundary. The EE of A can be calculated by the RT formula [66]

$$S = \frac{\text{Area}(\gamma_A)}{4G_N}, \quad (\text{A.1})$$

¹⁴Although there is no general argument, the mass square in all the models given in [40] is positive, and the absence of instabilities actually requires the positive mass square in MG and GA models [58, 63].

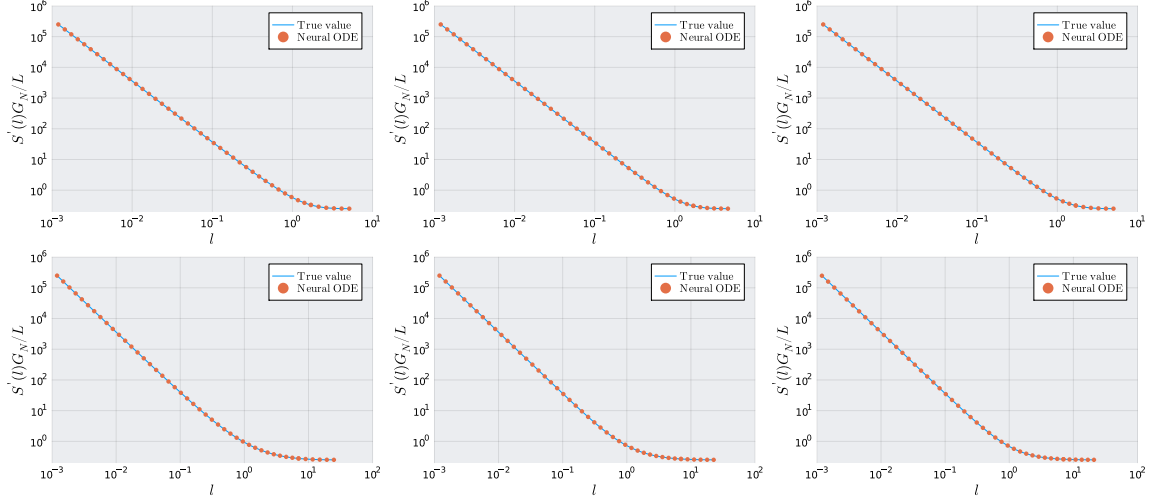


Figure 9: The performance of Neural ODEs in predicting $S'(l)$. From left to right, the three panels represent the results for the MG (left), LA (middle) and GA (right) models at high (top) and low (bottom) temperatures.

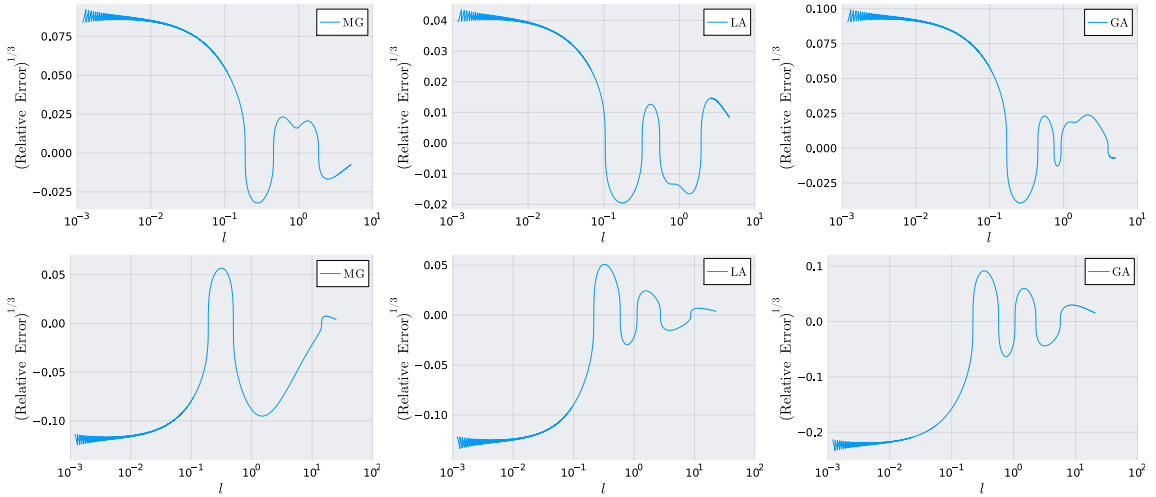


Figure 10: Relative errors in $S'(l)$ for three models at high (top) and low (bottom) temperatures.

where γ_A is the minimal surface in the bulk that is homologous to the boundary region A . Using the profile equation for γ_A , the EE and the width can be expressed as [11]

$$S(z_*) = \frac{L}{2G_N} \int_{\delta}^{z_*} \frac{z_*^2}{z^2 \sqrt{f(z)} \sqrt{z_*^4 - z^4}} dz, \quad (\text{A.2})$$

$$l(z_*) = 2 \int_0^{z_*} \frac{z^2}{\sqrt{f(z)} \sqrt{z_*^4 - z^4}} dz, \quad (\text{A.3})$$

where z_* is the radial coordinate at the tip of γ_A , and δ is the UV cutoff that is introduced

to avoid the divergence of EE. Comparing the derivatives of above two equations

$$\frac{dS(z_*)}{dz_*} = \frac{L}{2G_N} \left[\frac{1}{\sqrt{f(z_*)}} \lim_{z \rightarrow z_*} \frac{1}{\sqrt{z_*^4 - z^4}} - \int_0^{z_*} \frac{2z^2 z_*}{(z_*^4 - z^4)^{\frac{3}{2}} \sqrt{f(z)}} dz \right], \quad (\text{A.4})$$

$$\frac{dl(z_*)}{dz_*} = 2z_*^2 \left[\frac{1}{\sqrt{f(z_*)}} \lim_{z \rightarrow z_*} \frac{1}{\sqrt{z_*^4 - z^4}} - \int_0^{z_*} \frac{2z^2 z_*}{(z_*^4 - z^4)^{\frac{3}{2}} \sqrt{f(z)}} dz \right], \quad (\text{A.5})$$

where we have set $\delta \rightarrow 0$, one can obtain a simple formula

$$\frac{dS(l)}{dl} = \frac{L}{4G_N z_*^2}. \quad (\text{A.6})$$

With these preparations in place, let's substitute the bulk metric (the learned metric or the true value) into eq. (A.3) and get $l(z_*)$ by numerical integration. By the interpolation, we can construct the inverse function $z_*(l)$. In terms of eq. (A.6) with $z_*(l)$, the derivative $S'(l)$ can be obtained. In figure (9), we plot $S'(l)$ for the three models at (relatively) high temperatures and low temperatures. The change of the relative error along l is depicted in figure (10). Notably, the relative error decreases oscillatingly as l increases. At last, we calculate the MRE by uniformly sampling 10000 points within the allowed range of l , which are given in Table 3.

Model	MG	LA	GA
High temperature	1×10^{-5}	3×10^{-6}	2×10^{-5}
Low temperature	1×10^{-4}	1×10^{-5}	8×10^{-5}

Table 3: The MRE of $S'(l)$ for three models at two temperatures.

References

- [1] O. Aharony, S. S. Gubser, J. Maldacena, H. Ooguri and Y. Oz, *Large N field theories, string theory and gravity*, *Phys. Rep.* **323** (2000) 183. [[arXiv:hep-th/9905111](#)].
- [2] H. Liu and J. Sonner, *Quantum many-body physics from a gravitational lens*, *Nature Rev. Phys.* **2** (2020) 615. [[arXiv:2004.06159](#)].
- [3] T. De Jonckheere, *Modave lectures on bulk reconstruction in AdS/CFT*, *PoS Modave2017* (2018) 005. [[arXiv:1711.07787](#)].
- [4] D. Harlow, *TASI Lectures on the emergence of bulk physics in AdS/CFT*, *PoS TASI2017* (2018) 002. [[arXiv:1802.01040](#)].
- [5] N. Kajuri, *Lectures on bulk reconstruction*, *SciPost Phys. Lect. Notes* (2021) 22. [[arXiv:2003.00587](#)].
- [6] S. de Haro, S. N. Solodukhin and K. Skenderis, *Holographic reconstruction of space-time and renormalization in the AdS/CFT correspondence*, *Commun. Math. Phys.* **217** (2001) 595. [[arXiv:hep-th/0002230](#)].

- [7] J. Hammersley, *Extracting the bulk metric from boundary information in asymptotically AdS spacetimes*, *JHEP* **12** (2006) 047. [[arXiv:hep-th/0609202](#)].
- [8] V. E. Hubeny, H. Liu and M. Rangamani, *Bulk-cone singularities & signatures of horizon formation in AdS/CFT*, *JHEP* **01** (2007) 009. [[arXiv:hep-th/0610041](#)].
- [9] J. Hammersley, *Numerical metric extraction in AdS/CFT*, *Gen. Rel. Grav.* **40** (2008) 1619. [[arXiv:0705.0159](#)].
- [10] S. Bilson, *Extracting spacetimes using the AdS/CFT conjecture*, *JHEP* **08** (2008) 073. [[arXiv:0807.3695](#)].
- [11] S. Bilson, *Extracting Spacetimes using the AdS/CFT Conjecture: Part II*, *JHEP* **02** (2011) 050. [[arXiv:1012.1812](#)].
- [12] V. E. Hubeny, *Extremal surfaces as bulk probes in AdS/CFT*, *JHEP* **07** (2012) 093. [[arXiv:1203.1044](#)].
- [13] V. Balasubramanian, B. D. Chowdhury, B. Czech, J. de Boer and M. P. Heller, *Bulk curves from boundary data in holography*, *Phys. Rev. D* **89** (2014) 086004. [[arXiv:1310.4204](#)].
- [14] R. C. Myers, J. Rao and S. Sugishita, *Holographic holes in higher dimensions*, *JHEP* **06** (2014) 044. [[arXiv:1403.3416](#)].
- [15] B. Czech and L. Lamprou, *Holographic definition of points and distances*, *Phys. Rev. D* **90** (2014) 106005. [[arXiv:1409.4473](#)].
- [16] N. Engelhardt and G. T. Horowitz, *Towards a reconstruction of general bulk metrics*, *Class. Quant. Grav.* **34** (2017) 015004. [[arXiv:1605.01070](#)].
- [17] N. Engelhardt and G. T. Horowitz, *Recovering the spacetime metric from a holographic dual*, *Adv. Theor. Math. Phys.* **21** (2017) 1635. [[arXiv:1612.00391](#)].
- [18] S. R. Roy and D. Sarkar, *Bulk metric reconstruction from boundary entanglement*, *Phys. Rev. D* **98** (2018) 066017. [[arXiv:1801.07280](#)].
- [19] D. Kabat and G. Lifschytz, *Emergence of spacetime from the algebra of total modular Hamiltonians*, *JHEP* **05** (2019) 017. [[arXiv:1812.02915](#)].
- [20] K. Hashimoto, *Building bulk from Wilson loops*, *PTEP* **2021** (2021) 023B04. [[arXiv:2008.10883](#)].
- [21] K. Hashimoto and R. Watanabe, *Bulk reconstruction of metrics inside black holes by complexity*, *JHEP* **09** (2021) 165. [[arXiv:2103.13186](#)].
- [22] S. Caron-Huot, *Holographic cameras: An eye for the bulk*, *JHEP* **03** (2023) 047. [[arXiv:2211.11791](#)].
- [23] N. Jokela and A. Pönni, *Towards precision holography*, *Phys. Rev. D* **103** (2021) 026010 [[arXiv:2007.00010](#)].
- [24] N. Jokela, A. Pönni, T. Rindlisbacher, K. Rummukainen and A. Salami, *Disentangling the gravity dual of Yang-Mills theory*, *JHEP* **12** (2023) 137. [[arXiv:2304.08949](#)].
- [25] W. B. Xu and S. F. Wu, *Reconstructing black hole exteriors and interiors using entanglement and complexity*, *JHEP* **07** (2023) 083. [[arXiv:2305.01330](#)].
- [26] T. M. Nebabu and X. Qi, *Bulk reconstruction from generalized free fields*, [arXiv:2306.16687](#).
- [27] R. Q. Yang, *Inverse problem of correlation functions in holography and bulk reconstruction*, [arXiv:2310.10419](#).

- [28] K. Hashimoto, S. Sugishita, A. Tanaka and A. Tomiya, *Deep learning and the AdS/CFT correspondence*, *Phys. Rev. D* **98** (2018) 046019. [[arXiv:1802.08313](#)].
- [29] K. Hashimoto, S. Sugishita, A. Tanaka and A. Tomiya, *Deep learning and holographic QCD*, *Phys. Rev. D* **98** (2018) 106014. [[arXiv:1809.10536](#)].
- [30] T. Akutagawa, K. Hashimoto and T. Sumimoto, *Deep learning and AdS/QCD*, *Phys. Rev. D* **102** (2020) 026020. [[arXiv:2005.02636](#)].
- [31] K. Hashimoto, K. Ohashi and T. Sumimoto, *Deriving the dilaton potential in improved holographic QCD from the meson spectrum*, *Phys. Rev. D* **105** (2022) 106008. [[arXiv:2108.08091](#)].
- [32] Y. K. Yan, S. F. Wu, X. H. Ge and Y. Tian, *Deep learning black hole metrics from shear viscosity*, *Phys. Rev. D* **102** (2020) 101902(R). [[arXiv:2004.12112](#)].
- [33] K. Li, Y. Ling, P. Liu and M. H. Wu, *Learning the black hole metric from holographic conductivity*, *Phys. Rev. D* **107** (2023) 066021. [[arXiv:2209.05203](#)].
- [34] K. Hashimoto, H. Y. Hu and Y. Z. You, *Neural ODE and holographic QCD*, *Mach. Learn.: Sci. Technol* **2** (2021) 035011. [[arXiv:2006.00712](#)].
- [35] K. Hashimoto, K. Ohashi and T. Sumimoto, *Deriving dilaton potential in improved holographic QCD from chiral condensate*, *PTEP* **2023** (2023) 033B01. [[arXiv:2209.04638](#)].
- [36] B. Ahn, H. S. Jeong, K. Y. Kim and K. Yun, *Deep learning bulk spacetime from boundary optical conductivity*, [[arXiv:2401.00939](#)].
- [37] Ricky T. Q. Chen, Y. Rubanova, J. Bettencourt and D. Duvenaud. *Neural ordinary differential equations*. In: *Advances in Neural Information Processing Systems 31 (NeurIPS 2018)*. [[arXiv:1806.07366](#)].
- [38] K. Skenderis, *Lecture notes on holographic renormalization*, *Class. Quantum. Gravity* **19** (2002) 5849. [[arXiv:hep-th/0209067](#)].
- [39] I. Papadimitriou, *Lectures on holographic renormalization*, *Springer Proceedings in Physics Vol. 176: Theoretical frontiers in black holes and cosmology*, Springer Press (2016).
- [40] S. A. Hartnoll, D. M. Ramirez and J. E. Santos, *Entropy production, viscosity bounds and bumpy black holes*, *JHEP* **03** (2016) 170. [[arXiv:1601.02757](#)].
- [41] B. Bradlyn, M. Goldstein and N. Read, *Kubo formulas for viscosity: hall viscosity, ward identities, and the relation with conductivity*, *Phys. Rev. B* **86** (2012) 245309. [[arXiv:1207.7021](#)].
- [42] I. S. Burmistrov, et al., *Dissipative and hall viscosity of a disordered 2D electron gas*, *Phys. Rev. Lett.* **123** (2019) 026804. [[arXiv:1901.03561](#)].
- [43] M. Baggioli, S. Grieninger, and H. Soltanpanahi, *Nonlinear oscillatory shear tests in viscoelastic holography*, *Phys. Rev. Lett.* **124** (2020) 081601. [[arXiv:1910.06331](#)].
- [44] D. T. Son and C. Wu, *Holographic spontaneous parity breaking and emergent hall viscosity and angular momentum*, *JHEP* **07** (2014) 076. [[arXiv:1311.4882](#)].
- [45] J. Zaanen, Y. Liu, Y. W. Sun and K. Schalm, *Holographic duality in condensed matter*, Chapter 12, Cambridge University Press (2015).
- [46] K. M. He, X. Y. Zhang, S. Q. Ren and J. Sun. *Deep residual learning for image recognition*. In: *2016 IEEE Conference on Computer Vision and Pattern Recognition (CVPR)* **770** (2016). [[arXiv:1512.03385](#)].

- [47] L. S. Pontryagin, E. F. Mishchenko, V. G. Boltyanskii and R. V. Gamkrelidze, *The mathematical theory of optimal processes*, 1962.
- [48] P. F. Chen, G. Y. Chen and S. Y. Zhang, *Log hyperbolic cosine loss improves variational auto-encoder*, 2018.
- [49] Q. Wang, Y. Ma, K. Zhao and Y. J. Tian, *A comprehensive survey of loss functions in machine learning*, *Ann. Data. Sci.* **9** (2020) 187.
- [50] X. Xu, J. Li, Y. Yang and F. M. Shen, *Toward effective intrusion detection using log-cosh conditional variational autoencoder*, *IEEE Internet of Things Journal* **8** (2021) 6187.
- [51] Resve A. Saleh and A. K. Md. Ehsanes Saleh, *Statistical properties of the log-cosh loss function used in machine learning*, [[arXiv:2208.04564](https://arxiv.org/abs/2208.04564)].
- [52] Jorge Nocedal and Stephen J. Wright. *Quasi-Newton methods*. In: *Numerical Optimization* **135, 3** Springer New York (2006).
- [53] M. Fierz and W. Pauli, *On relativistic wave equations for particles of arbitrary spin in an electromagnetic field*, *Proc. Roy. Soc. Lond.* **173** (1939) 211.
- [54] H. van Dam and M. J. Veltman, *Massive and mass-less Yang-Mills and gravitational fields*, *Nucl. Phys. B* **22** (1970) 397.
- [55] V. I. Zakharov, *Linearized gravitation theory and the graviton mass*, *JETP Lett.* **12** (1970) 312.
- [56] A. I. Vainshtein, *To the problem of nonvanishing gravitation mass*, *Phys. Lett. B* **39** (1972) 393.
- [57] D. G. Boulware and S. Deser, *Can gravitation have a finite range?* *Phys. Rev. D* **6** (1972) 3368.
- [58] D. Vegh, *Holography without translational symmetry*, [[arXiv:1301.0537](https://arxiv.org/abs/1301.0537)].
- [59] C. de Rham and G. Gabadadze, *Generalization of the Fierz-Pauli action*, *Phys. Rev. D* **82** (2010) 044020. [[arXiv:1007.0443](https://arxiv.org/abs/1007.0443)].
- [60] C. de Rham, G. Gabadadze and A. J. Tolley, *Resummation of massive gravity*, *Phys. Rev. Lett.* **106** (2011) 231101. [[arXiv:1011.1232](https://arxiv.org/abs/1011.1232)].
- [61] C. de Rham, *Massive gravity*, *Living Rev. Relativity* **17** (2014) 7. [[arXiv:1401.4173](https://arxiv.org/abs/1401.4173)].
- [62] T. Andrade and B. Withers, *A simple holographic model of momentum relaxation*, *JHEP* **05** (2014) 101. [[arXiv:1311.5157](https://arxiv.org/abs/1311.5157)].
- [63] M. Baggioli and O. Pujolas, *Holographic polarons, the metal-insulator transition and massive gravity*, *Phys. Rev. Lett.* **114** (2015) 251602. [[arXiv:1411.1003](https://arxiv.org/abs/1411.1003)].
- [64] M. Baggioli, K. Y. Kim, L. Li and W. J. Li, *Holographic axion model: a simple gravitational tool for quantum matter*, *Sci. China Phys. Mech. Astron.* **64** (2021) 270001. [[arXiv:2101.01892](https://arxiv.org/abs/2101.01892)].
- [65] D. Pan, T. Ji, M. Baggioli, L. Li and Y. Jin, *Non-linear elasticity, yielding and entropy in amorphous solids*, *Sci. Adv.* **8** (2022) eabm8028. [[arXiv:2108.13124](https://arxiv.org/abs/2108.13124)].
- [66] S. Ryu and T. Takayanagi, *Holographic derivation of entanglement entropy from AdS/CFT*, *Phys. Rev. Lett.* **96** (2006) 181602. [[hep-th/0603001](https://arxiv.org/abs/hep-th/0603001)].
- [67] L. Altenkort, et al., *Viscosity of pure-gluon QCD from the lattice*, *Phys.Rev.D* **108** (2023) 014503. [[arXiv:2211.08230](https://arxiv.org/abs/2211.08230)].

- [68] F. Turro, A. Ciavarella, and X. Yao, *Classical and quantum computing of shear viscosity for 2+1D SU(2) gauge theory*, *Phys.Rev.D* **109** (2024) 114511. [[arXiv:2402.04221](#)].
- [69] H. Y. Hu, S. H. Li, L. Wang and Y. Z. You, *Machine learning holographic mapping by neural network renormalization group*, *Phys. Rev. Res.* **2** (2020) 023369. [[arXiv:1903.00804](#)].
- [70] X. Han and S. A. Hartnoll, *Deep quantum geometry of matrices*, *Phys. Rev. X* **10** (2020) 011069. [[arXiv:1906.08781](#)].
- [71] J. Lam and Y. Z. You, *Machine learning statistical gravity from multi-region entanglement entropy*, *Phys. Rev. Res.* **3** (2021) 043199. [[arXiv:2110.01115](#)].
- [72] Y. Z. You, Z. Yang and X. L. Qi, *Machine learning spatial geometry from entanglement features*, *Phys. Rev. B* **97** (2018) 045153. [[arXiv:1709.01223](#)].
- [73] F. Chen, S. F. Wu and Y. X. Peng, *Hamilton-Jacobi approach to holographic renormalization of massive gravity*, *JHEP* **07** (2019) 072. [[arXiv:1903.02672](#)].
- [74] M. X. Ma and S. F. Wu, *Holographic renormalization in the Hamilton-Jacobi formulation with exact ansatz generation*, *Phys. Rev. D* **107** (2023) 066012. [[arXiv:2208.10012](#)].
- [75] S. A. Hartnoll, C. P. Herzog, G. T. Horowitz, *Building an AdS/CFT superconductor*, *Phys. Rev. Lett.* **101** (2008) 031601. [[arXiv:0803.3295](#)].
- [76] M. Geracie, D. T. Son, C. Wu and S. F. Wu, *Spacetime symmetries of the quantum hall effect*, *Phys. Rev. D* **91** (2015) 045030. [[arXiv:1407.1252](#)].
- [77] C. Tsitouras, *Runge-Kutta pairs of orders 5(4) satisfying only the first column simplifying assumption*, *Computers and Mathematics with Applications* **62** (2011) 770.
- [78] S. Arlot and A. Celisse, *A survey of cross-validation procedures for model selection*, *Statistics Surveys* **4** (2010) 40. [[arXiv:0907.4728](#)].
- [79] C. Ran, Z. Y. Xian, and S. F. Wu, in progress.
- [80] E. Hairer and G. Wanner, *Stiff differential equations solved by radau methods*, *J. Comput. Appl. Math.* **111** (1999) 93.